C. R. Mecanique 347 (2019) 685–700

Contents lists available at ScienceDirect

Comptes Rendus Mecanique

www.sciencedirect.com

Energy consumed by a bearing supported spindle in the presence of a dynamic cutting force and of defects

Anoire Ben Jdidia [a,b,*], Taissir Hentati [a], Alain Bellacicco [b], Mohamed Taoufik Khabou [a], Alain Riviere [b], Mohamed Haddar [a]

[a] Laboratoire de recherche de mécanique, modélisation et productique (LA2MP), Université de Sfax, École nationale d'ingénieurs de Sfax, route de la Soukra km 4, 3038 Sfax, Tunisia
[b] Laboratoire Quartz, Institut supérieur de mécanique de Paris (SUPMECA), 3, rue Fernand-Hainaut, 93400 Saint-Ouen cedex, France

ARTICLE INFO

Article history:
Received 29 May 2018
Accepted 14 September 2019
Available online 9 October 2019

Keywords:
Dynamic behavior
Cutting forces
Rolling bearings
Spindle consumed power
Rolling defects
Mounting faults

ABSTRACT

A machine tool spindle system model is proposed in this paper to investigate the non-linear face-milling cutting forces behavior, which are neglected in the literature, in order to predict the total mechanical power of a spindle. A simulation of the structure of the spindle based on the finite-element method is elaborated to estimate the variable cutting forces and then the variable power loss generated by bearings, considering the angular position and contact angles of the variable balls. Experiments are elaborated to compare the experimental power values with the predicted results. Particular attention is paid to different types of defects (inner ring spalling, outer ring spalling, eccentricity, and unbalance) in order to study their impact on the power consumed by the spindle during the approach and cutting phases under different rotating conditions.

1. Introduction

During the manufacturing process, machine tools are major consumers of a significant amount of electrical energy [1–4]. For example, in the USA, quite half of the total electricity consumption due to manufacturing is attributable to machine tools electricity consumption as mentioned by Zhou [2]. According to He [5], the efficiency of the machining processes is below 30%. Kant [6] and Li [7] show that 99% of the environmental impacts are caused by the milling and turning processes. This is why the reduction of energy consumption by machine tool is an important challenge for sustainable manufacturing [8] and attract the attention of industrials and academic researchers. According to Hu [9] and Jia [10], machine tool energy modelling is decisive for the prediction of energy consumption. During manufacturing, the spindle system consumes the majority of the machine tool energy, which varies instantly according to the nature of the manufacturing operations [11]. As mentioned by Dietmair [12], more than 15% of the total energy can be consumed by the spindle system, leading the investigators to focus on it due to its important role in machine tool energy consumption [13]. For this reason, the energy required by the spindle system must be understood and analyzed [14].

In order to analyze the energy consumed by the spindle system, several research works have been performed. We can cite a mathematical model proposed by Avram [15], in which he computes the power consumed during the spindle revolution

* Corresponding author at: Laboratoire Quartz, Institut supérieur de mécanique de Paris (SUPMECA), 3, rue Fernand-Hainaut, 93400 Saint-Ouen cedex, France.
E-mail address: anoire.ben-jdidia@supmeca.fr (A. Ben Jdidia).

https://doi.org/10.1016/j.crme.2019.09.002
1631-0721/

in the transient phases, such as the acceleration and the deceleration, as well as the steady-state phase during cutting. The author approach consists in computing the spindle energy by multiplying the useful torque by the angular velocity. The useful torque is obtained from the cutting speed and the cutting forces measured from the experimental situation during the steady and variable states. In his model, the author uses the obtained useful torque to compensate for the cutting torque and the mechanical friction torque caused by the bearings' revolution. In this work, the tangential cutting force component is considered constant by neglecting its dynamic behavior caused by the chip thickness variation in the real milling process. Furthermore, the power loss of the bearings is considered constant, while the balls' angular position and contact angles change with time during turning.

The specific cutting force and the NC code information, which implies too high estimation errors, is used by He [5] to evaluate the spindle's cutting energy demand.

An empirical model to estimate the energy consumption by the spindle system has been developed by Lv [16] and Hu [9]. The spindle system's energy is defined as the sum of both the energy required to make the spindle rotate during the air cutting motions, and the energy required to remove material during a face milling process. This latter energy is estimated using the empirical cutting force proposed by Ai [17].

An amelioration of the Lv [16] model is proposed by Deng [18]. The authors include a power loss coefficient in the empirical formula giving the power required by the spindle to compensate for the electrical and the mechanical loss, as assumed by Li [19]. In fact, the electrical and mechanical power loss in the motor and the transmission systems are introduced in the total cutting power. This quantity is expressed as a quadratic function of the cutting power and is obtained experimentally.

Response Surface Methodology (RSM) is used by Draganescu [20] to model the required tangential cutting force. This force is used to estimate the Specific Cutting Energy (SCE) consumed by the spindle system during a face − milling operation. The proposed SCE model, based on experiments, takes into account the relationship between the energy of the tool tip and the major machining parameters. Consequently, it is possible to study the influence of the machining parameters and of the tangential cutting force on the energy efficiency only for the studied case (same machine, same tool, and same workpiece material). The power required by the spindle during the transient state is neglected.

Some authors [16,18,9,19,20] have computed the empirical cutting force as a generic exponential model of the cutting parameters. Various model coefficients have been determined using a regression analysis (through several laborious and costly experiments). In these investigations, the cutting force is modeled without taking into account its dynamic nature during the milling process. By consequence, the power demand of the spindle revolution during the cutting phase was assumed to be constant and was not explicitly modeled, although the spindle system is described by Rief [21] as a dynamic consumer of energy.

According to Rief [21], the power required by the spindle system is comprised of two parts: an idle power (air-cutting power) presented as a function of the spindle speed, and a removing material power, which represents the mechanical losses. The cutting power, calculated by dividing the removal rate of the material by the removal rate of the specific material, has been modelled without consideration of the variation over time of the cutting section, which intervenes in the formation of the chip thickness. One can conclude that this static domain, which neglects the temporal parameter used by the authors to model the cutting force and predict the demanded spindle power, is suitable only for turning operations where the cutting section and the conditions of contact between the tool and the workpiece are constant.

The spindle system power model, for a three-axis milling machine, has been split by Peng [14] into the power required to make the spindle rotate during the unloading phase at various speeds and the power needed for removing the material obtained by a multiple regression. This empirical model needs laborious and costly experiments to collect the power data used afterwards to determine the unknown coefficients by a regression analysis.

To determine the spindle motor consumed power, Borgia [22] proposed a model composed of two parts, such as the mechanical output power and the Joule losses caused by the stator winding resistances. The spindle mechanical torque is used to accelerate the spindle, to overcome the cutting torque, and to compensate for the system frictions. The cutting force formulation considers the shear of the material as well as the friction contact area between the workpiece surface and the tool flank face.

Edem [23] grouped the power demanded by the spindle into the power required to make the spindle rotate at specified speeds and the one required for the motion tool tip in the milling operation based on the multiplication of the specific cutting pressure by the material removal rate. Lv [24] proposed a model for the turning machine during a phase of material removing taking into account the energy lost in the mechanical transmission system. These authors have based their estimation of the power loss on the quadratic function of the cutting force.

All those studies are recapitulated and discussed in Table 1, from which we can conclude that the dynamic behavior of the machining system has been neglected in the investigations cited above, in which chip thickness was assumed to be constant during the milling operation. Also, the frictional power lost by the bearings is either neglected or expressed as an empirical function or coefficient, except in Avram's [15] model, where the temporary behavior of the rolling bearings is neglected. We note also that the impact of the bearings' defects on power consumption by the spindle has not been treated. The objective of this paper is to consider the dynamic behavior of both the cutting force (chip thickness temporal variation) and the bearings' load. Different types of defects are also taken into consideration in this investigation. This strategy will surely lead to a better understanding of the factors impacting the energy demand by the spindle system and consequently will help the manufacturers to plan operations with lower energy consumption. A numerical model, taking into account

Table 1
Recapitulation of the results of various authors.

Models computing	Authors	Approach	Remarks
Cutting power	He [12]	Specific cutting force based on NC code information	The dynamic behavior of the cutting force is neglected
	Lv [16] + Hu [9]	Empirical model of the cutting force computed from an experimental situation	
	Draganescu [20]	Empirical model of the cutting force computed from an experimental situation	
	Peng [14]	Empirical model of the cutting force computed from an experimental situation	
	Borgia [22]	Analytical constant cutting force	
	Rief [21]	Analytical constant cutting force	
Power loss of the bearings	Lv [24]	Empirical constant cutting force	The distribution of the contact efforts of the balls is considered constant
Cutting energy and power loss of the bearings	Avram [15]	Constant cutting force computed from an experimental situation A constant distribution of the effort of the balls is considered	The dynamic behavior of the cutting force is neglected
	Li [19]	Empirical model of the cutting force computed from an experimental situation	
	Deng [18]	Empirical model of the cutting force computed from an experimental situation An empirical coefficient is introduced to consider the electrical and mechanical power loss computed from an experimental situation	The distribution of the contact efforts of the balls is constant

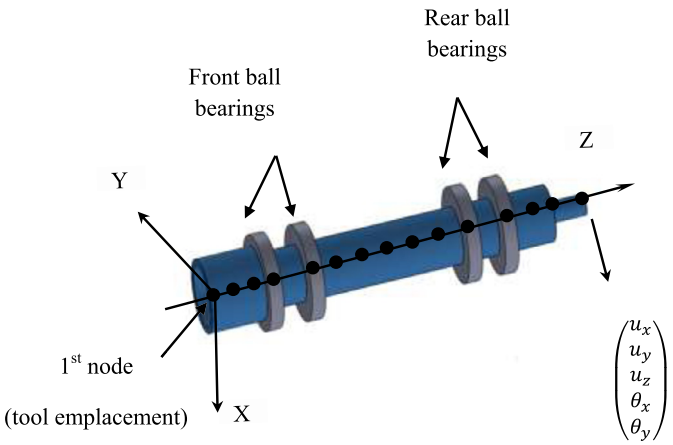

Fig. 1. Schematic representation of the spindle system.

the dynamic behavior of the cutting force and the bearings force is developed. The obtained results are compared with the experiments in order to illustrate the theoretical approach. A parametric study is performed, showing the variation with different machining parameters of the power and the energy consumed by the spindle. In the second step we introduce different bearings defect (mounting and wear defects) in order to show their impacts on the spindle energy consumption.

2. Experimental study

A CNC FEELER fv-760 cutting machine is used to perform an experimental study. The associated spindle is displayed in Fig. 1, and the characteristics of the machine are given in Table 2. The used mild steel workpiece is 150 mm in length, 100 mm in width, and 50 mm in thickness.

The physical diagram in Fig. 2 shows the connection of the three voltage and current probes with the spindle system's drive measuring real-time signals.

The two NI-9223 data-collecting cards are involved in the analog-to-digital signal conversion and the setup of the experimental instrumentation of the studied machine tool is shown in Fig. 3. Signal recording is carried out using a NI cDAQ-9174 device. Otherwise, the LabVIEW interface is used for data processing in order to acquire and to analyse the instantaneous power consumed by a spindle system. The measured mechanical power is obtained by subtracting the Joule power from the total absorbed one according to the following equation:

Table 2
Machine tool characteristics.

Maximum feed system cross travel along the Z axis	510 mm
Spindle diameter	80 mm
Tool holder	BT 40
Machine speed	50–8000 rpm
Bearings type	SKF 6016-2Z
Column–spindle axis	665 mm

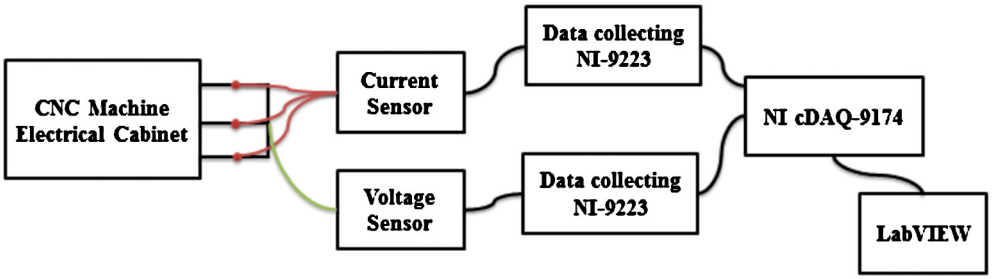

Fig. 2. Physical diagram showing the cabling.

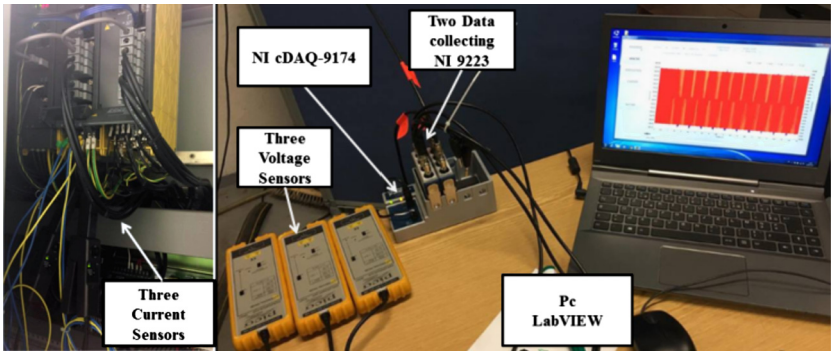

Fig. 3. Wiring schema.

$$P_{\text{mechanical}} = P_{\text{absorbed}} - P_{\text{Joule}} \tag{1}$$

with

$$P_{\text{Joule}} = R(I_0^2 + I_1^2 + I_2^2) \tag{2}$$

where $R = 2.42\ \Omega$ is the motor resistance measured by a multimeter and I_0, I_1, and I_2 are the values of the current per phase.

The experimental evolution of the mechanical power consumed by the spindle system during a single pass of face milling using a cutting speed of 140 m/min, an axial depth of cut of 2 mm, and a feed per tooth of 0.1 mm/tooth is shown in Fig. 4.

The spindle power curve showed above varies according the different machining stages. A transient state is shown in the first zone with a short duration and is characterized by a power peak which is highly intense in energy; it represents the start-up of the spindle from zero to the given rotational speed. The second zone, called the approach phase, represents the air-cutting phase, where the spindle system's mechanical transmission consumes an unloaded power when no load is applied to the cutting tool. The third phase describes the cutting phase, where the teeth are engaged in the workpiece to remove the material. This phase is divided into three zones: two short zones defining the engagement and the disengagement of the tool. The long zone corresponds to a stationary cutting phase, in which the tool is totally engaged to remove material. As shown in this zone, the spindle power is not static, but dynamic, throughout a face milling pass. During this phase, the spindle motor consumes the net cutting power needed for material removal and the mechanical power loss of the bearings.

We are interested in this paper in studying the dynamic behavior of the consumed power and energy during the stationary cutting phase. The operation consists of a single-pass face-milling removing material for a low rotational speed (716 and 1115 rpm).

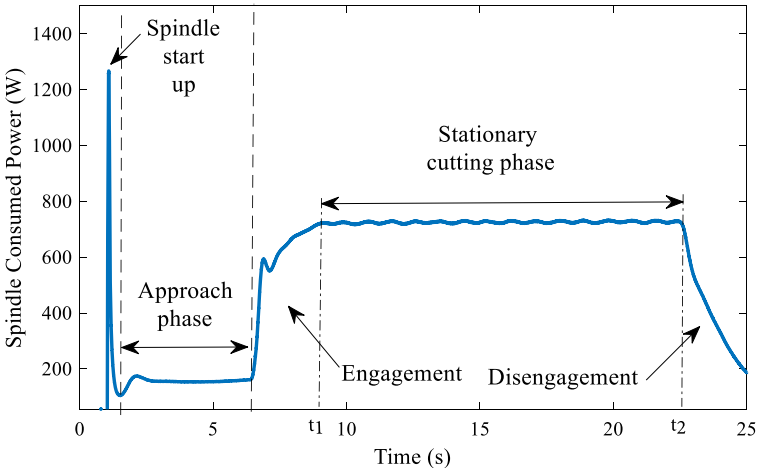

Fig. 4. Experimental curve giving the spindle power.

3. Spindle cutting power and energy modelization

For a given spindle system, the consumed cutting energy can be calculated as follows:

$$E_{\text{spindle}-\text{theoretical}} = \int_{t_1}^{t_2} P_{\text{cutting}}\,\mathrm{d}t \tag{3}$$

where t_1 and t_2 denotes the beginning and the ending time of the stationary cutting phase (tool totally engaged), and P_{cutting} is the consumed cutting power. This power is written as the sum of the removing material power $P_{\text{material removal}}$ (the power consumed caused by the cutting operation) and of the required power to compensate for the bearings losses P_{bearings}:

$$P_{\text{cutting}}(t) = P_{\text{material removal}}(t) + P_{\text{bearings}}(t) \tag{4}$$

In the next sections, we define these two powers.

3.1. Removing material power modelling

The removing material power of the spindle has been expressed by Avram [15] as:

$$P_{\text{material removal}} = \frac{F_{\text{t}} V_{\text{c}}}{60} \tag{5}$$

where V_{c} represents the cutting speed and F_{t} is the tangential cutting force considered constant in Avram's [15] approach, but variable in this study. This assumption is justified by Fig. 4, where the spindle system's cutting power zone follows a dynamic behavior. In fact, the vibration of the tool during an operation of face-milling material removing between the present and the previous tooth produce a dynamic chip thickness component added to a statical one, which affects the magnitude of the cutting forces.

In order to quantify this dynamic tangential cutting force, we solve the system of motion equations [25]. The Finite Element Method (FEM) was used to descritize the spindle to 15 linear elements using Timoshenko's theory. Each node has five degrees of freedom, as shown in Fig. 1:

$$\begin{aligned}&\left[M_E\right]\left\{\ddot{u}\right\} + 2\Omega\left[G_E\right]\left\{\dot{u}\right\} \\ &\quad + \left(\left[K_E\right] - \Omega^2\left[C_E\right]\right)\left\{u\right\} = F_c(t,u) + \textstyle\sum_{i=1}^{N}\sum_{j=1}^{N_b} F_{j\ \text{in/ou}}(t,u)\end{aligned} \tag{6}$$

where $[M_E]$, $[G_E]$, $[K_E]$ and $[C_E]$ represent respectively the mass, the gyroscopic, the rigidity and the centrifuge matrices, Ω (rad/s) represents the spindle's angular speed.

The effect of the bearings is introduced in the second member $\sum_{i=1}^{N}\sum_{j=1}^{N_b} F_{j\ \text{in/ou}}$ as well as the cutting force F_{c}, which is written in the associated spindle coordinate frame (Fig. 1) using the instantaneous tangential cutting force $F_{\text{t}}(t)$, the instantaneous radial cutting force $F_{\text{r}}(t)$, and the instantaneous axial cutting force $F_{\text{a}}(t)$, calculated for each tooth as follows:

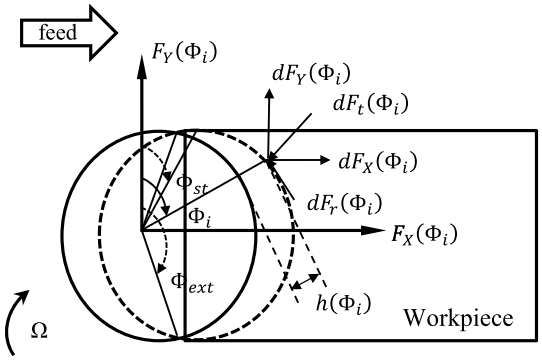

Fig. 5. Face milling geometry [26].

$$F_c = \sum_{i=1}^{N} \begin{Bmatrix} dF_X(\Phi_i(t)) \\ dF_Y(\Phi_i(t)) \\ dF_Z(\Phi_i(t)) \end{Bmatrix} = \sum_{i=1}^{N} \begin{bmatrix} -\cos(\Phi_i(t)) & -\sin(\Phi_i(t)) & 0 \\ \sin(\Phi_i(t)) & -\cos(\Phi_i(t)) & 0 \\ 0 & 0 & 1 \end{bmatrix} \begin{Bmatrix} dF_t(\Phi_i(t)) \\ dF_r(\Phi_i(t)) \\ dF_a(\Phi_i(t)) \end{Bmatrix} \tag{7}$$

where $\Phi_i(t)$ is the instantaneous angular position of the ith tooth written using the spindle's angular velocity Ω and the tooth number N as:

$$\Phi_i(t) = \Omega t + (i-1)\frac{2\pi}{N} \tag{8}$$

and dF_t, dF_r, and dF_a define respectively the elementary instantaneous tangential, radial, and axial cutting force components displayed in Fig. 5.

These tangential, radial and axial elementary cutting forces are written as (Budak [27]):

$$dF_t(t) = g(\Phi_i(t))k_t a_p h(\Phi_i(t)) \tag{9}$$

$$dF_r(t) = k_r dF_t(t) = k_r g(\Phi_i(t))k_t a_p h(\Phi_i(t)) \tag{10}$$

$$dF_a(t) = k_a dF_t(t) = k_a g(\Phi_i(t))k_t a_p h(\Phi_i(t)) \tag{11}$$

where k_t, k_r and k_a are coefficients of the cutting force assumed to be constant and a_p is the axial depth of cut, while $h(\Phi_i(t))$ is the chip load, which can be written, for a single-pass face-milling operation, as:

$$h(\Phi_i(t)) = f_z \sin(\Phi_i(t)) + (u_X(t) - u_X(t-\tau))\sin(\Phi_i(t)) + (u_Y(t) - u_Y(t-\tau))\cos(\Phi_i(t)) \tag{12}$$

with f_z is the feed per tooth, $u_X(t)$ and $u_Y(t)$ are the tool tip displacements at the present time according to, respectively, the cutting force excitation of the spindle structure in the feed direction (X) and the normal to the feed direction (Y), whereas the tool tip displacements at previous times are $u_X(t-\tau)$ and $u_Y(t-\tau)$; τ is the period time of two teeth and is described as a function of the angular speed of the spindle Ω (rad/s) as follows:

$$\tau = \frac{2\pi}{\Omega N} \tag{13}$$

$g(\Phi_i(t))$ is a function defining the tooth-workpiece engagement. It describes whether the ith tooth is out or in the cutting process; it is written as:

$$g(\Phi_i(t)) = \begin{cases} 1 & \text{if } \Phi_{st} < \Phi_i(t) < \Phi_{ext} \\ 0 & \text{otherwise} \end{cases} \tag{14}$$

where Φ_{st} and Φ_{ext} are respectively the cutter entry and exit angles (Fig. 5).

The equation of motion is resolved using Newmark's method coupled with the Newton–Raphson method. The time step considered in our study in expressed as a function of the spindle rotational speed. It is equal to the spindle's rotational speed divided by 1000 (number of iterations allowing the passage from the first tooth to the next one). The Newmark's coefficients are both equal to 0.25. During the first tooth passage, the delay term is neglected and the value of the displacement $u_X(t-\tau)$ and $u_Y(t-\tau)$ is stocked. An update of these values is thereafter relayed until the end of the simulation. The computed tangential component of the cutting force $F_t = \sum_{i=1}^{N} dF_t$ is then used to determine the removing material power (Eq. (5)).

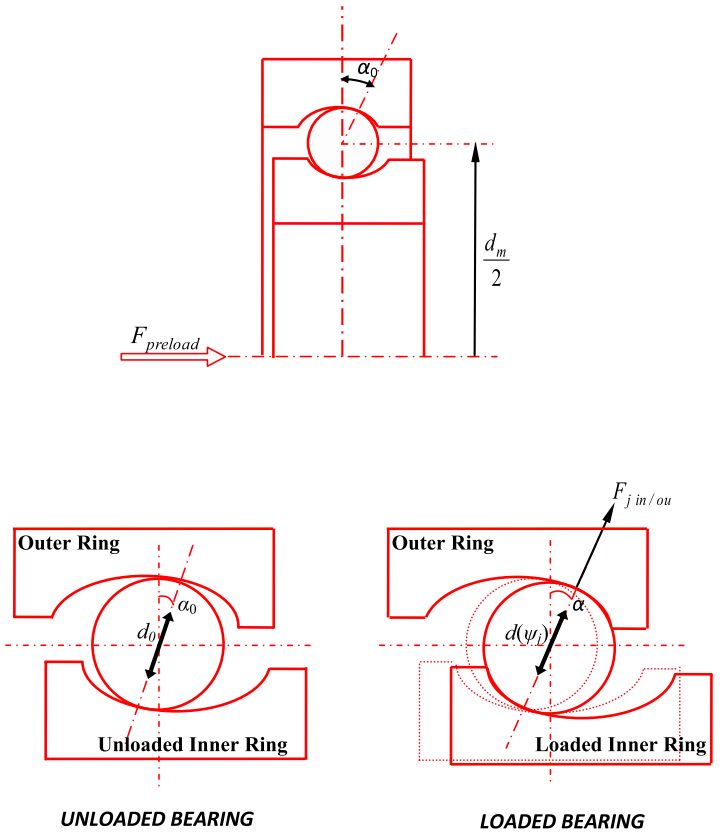

Fig. 6. Parameters of the bearing.

3.2. Bearing power loss modelling

In our study, we used the Avram approach [28] to compute the power losses of the bearings. In fact, we used the formula given by Avram [28] to compute the bearings' torques. But, in our study, we suppose that the distribution of the load of the bearings is variable with time and the contact angles of the balls are also variable when the spindle is turning, while Avram's [28] approach considers those two parameters as constants.

The power required to compensate for the bearing frictions for one bearing is expressed by Avram [28] as follows:

$$P_{\text{bearing}} = 1.047 \times 10^{-4} \frac{30\Omega}{\pi} (T_{\text{load}} + T_{\text{spin}} + T_{\text{vis}}) \tag{15}$$

with T_{load}, T_{spin}, T_{vis} are respectively the load, the spin and the viscosity related torque considered by our approach as functions of time.

The load related torque T_{load} is expressed using the total axial cutting force $F_{\text{a}}(t) = \sum_{i=1}^{N} \mathrm{d}F_{\text{a}}$ and total radial cutting force $F_{\text{r}}(t) = \sum_{i=1}^{N} \mathrm{d}F_{\text{r}}$ given by Eqs. (10) and (11). The load-related torque can be written as:

$$T_{\text{load}}(t) = z\left(\frac{x_{\text{s}} F_{\text{r}}(t) + y_{\text{s}}(F_{\text{a}}(t) + F_{\text{preload}})}{C_{\text{s}}}\right)^{y} + \left(\max\left(0.9(F_{\text{a}}(t) + F_{\text{preload}})\cot(\alpha) - 0.1F_{\text{r}}(t), F_{\text{r}}(t)\right)\right) d_{\text{m}} \tag{16}$$

where $d_{\text{m}} = 92$ mm is the bearings' pitch diameter, $\alpha = 30^{\circ}$ is the contact angle in degree and F_{preload} is the bearing preloading force used to improve the stiffness of the bearing and to guarantee the proper bearing-raceway contact as given by Fig. 6. We note that F_{preload} is considered null in our modelling.

x_{s} and y_{s} are respectively the radial and axial factors depending on the bearing type. For a bearing having a single row and a contact angle equal to 30°, we choose $x_{\text{s}} = 0.5$ and $y_{\text{s}} = 0.33$ [28].

$z = 0.001$ and $y = 0.33$ are constants chosen according to the bearing type and $C_{\text{s}} = 48964.16N$ is the load-rating factor [28].

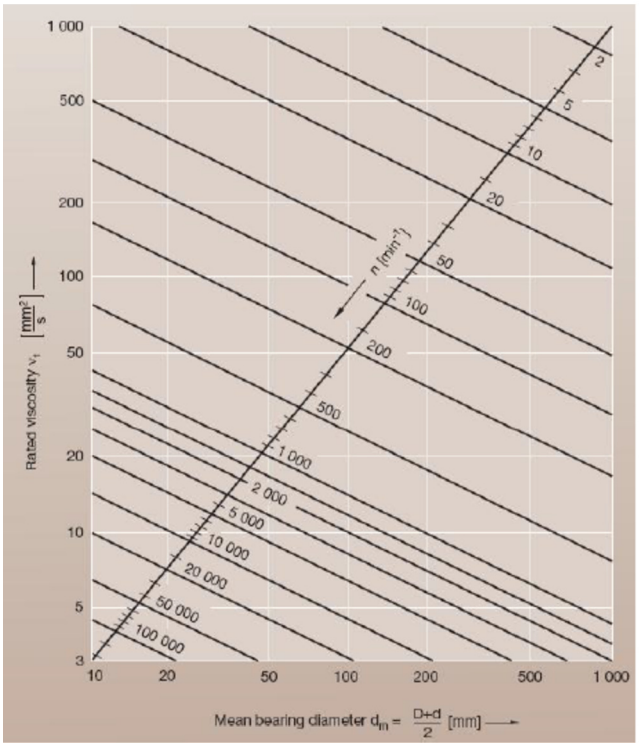

Fig. 7. Viscosity values [29].

The spin related torque T_{spin} can be written as follows:

$$T_{\text{spin}}(t) = \sum_{j=1}^{N_b} \frac{3\mu_b F_{j\ \text{in/ou}}(t) a_{\text{in/ou}}(t) \epsilon_{\text{in/ou}}}{8} \tag{17}$$

with

$$a_{\text{in/ou}}(t) = 0.0236 \times a^*_{\text{in/ou}} \frac{F_{j\ \text{in/ou}}(t)}{\sum \rho_{\text{in/ou}}} \tag{18}$$

where $N_b = 23$ is the number of balls of the bearings, $\mu_{\text{b}} = 0.005$ is the friction coefficient, $a^*_{\text{in/ou}} = 2.8$, $\epsilon_{\text{in/ou}} = 1.01$, and $\sum \rho_{\text{in/ou}} = 0.16$ are the coefficients of the ball [28].

The normal force applied by the rolling element on the inner ring $F_{j\ \text{in/ou}}(t)$ (Fig. 6) is calculated during the resolution of the equation of motion Eq. (6). It is written as:

$$F_{j\ \text{in/ou}}(t) = k_{\text{p}} \Delta_j^{1.5} \tag{19}$$

where k_{p} is the Hertz constant and Δ_j is the jth ball contact deflection written as a function of the loaded $d(\psi_j)$ and unloaded d_0 distances between the inner and outer rings curvature centres (Fig. 6), written as:

$$\Delta_j = d(\psi_j(t)) - d_0 \tag{20}$$

The loaded distance between the inner and outer rings curvatures centres can be written as a function of the radial and axial jth ball deflections (written as a function of the degrees of freedom of the bearings' node) and of the jth ball angular position $\psi_j(t)$ (Fig. 13).

According to Avram [28], the viscosity related torque T_{visc} can be expressed as:

$$T_{\text{vis}} = \begin{cases} 10^{-7} f_0 (\nu_{\text{oil}} \frac{30\Omega}{\Pi})^{2/3} d_{\text{m}} & \text{if } \nu_{\text{oil}} \frac{30\Omega}{\Pi} \geq 2000 \\ 160 \times 10^{-7} f_0 d_{\text{m}}^3 & \text{if } \nu_{\text{oil}} \frac{30\Omega}{\Pi} \leq 2000 \end{cases} \tag{21}$$

where $f_0 = 1.7$ is the bearing type factor and ν_{oil} is the kinematic viscosity of the oil.

In order to determine the viscosity values, we used Fig. 7 [29]:

For a cutting velocity equal to 140 m/min or to 90 m/min, we can deduce a kinematic viscosity equal to 18 or 25, respectively. The different steps to compute the cutting energy are summarized in the next flowchart.

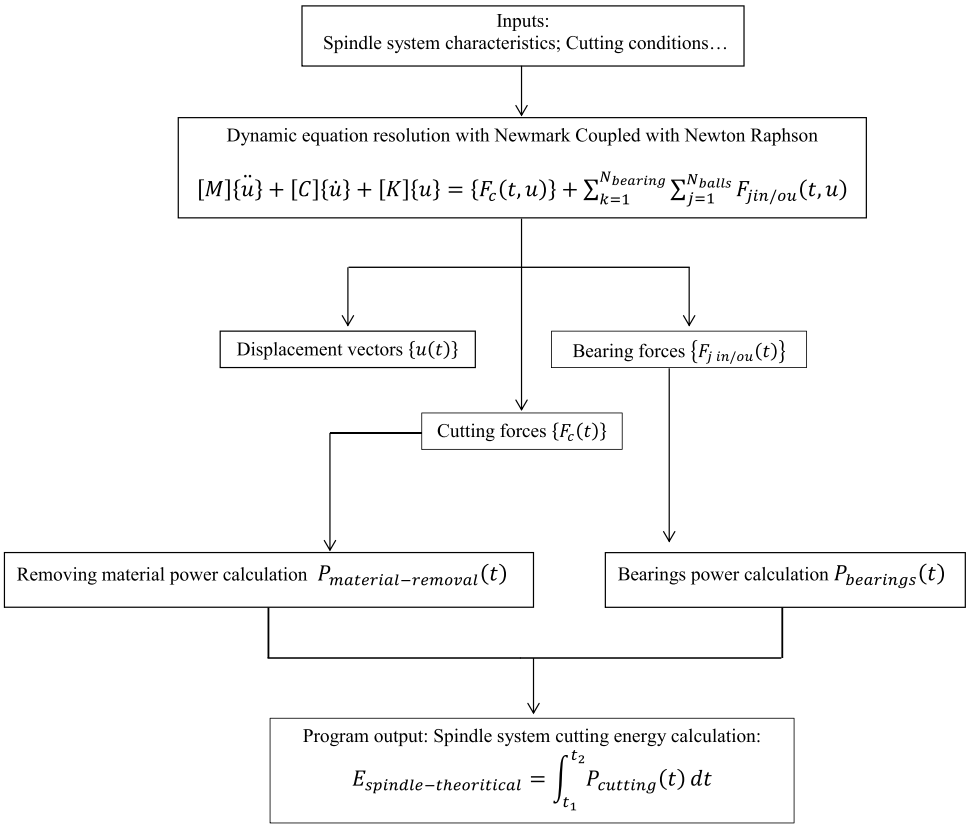

Fig. 8. Flowchart of the cutting energy compilation.

Table 3
The different specific pressures of the cutting tool.

Specific pressure of the cutting tool along	Values (N/mm^2)
Tangential direction k_t	2200
Radial direction k_r	0.8
Axial direction k_a	0.7

4. Results and discussion

The different specific pressures of the cutting tool are recapitulated in Table 3, and the cutting energy and power are calculated using the flowchart in Fig. 8. Our study is performed for a single-pass face-milling operation with the same cutting parameters as in Fig. 4.

We focused, in a first time, on the consumed cutting power magnitude, given by the experimental in situ method and the numerical one. A comparison between the computed and experimental results is performed in terms of minimum, maximum, and mean average values. The obtained results are given in Fig. 9. We note a good agreement between the experimental and computed results. In fact, the errors between the computed and experimental values of the consumed power are respectively 5.72%, 2.18%, and 3.36% (minimum, maximum, and mean average, respectively).

In order to illustrate the proposed model, we have compared the variation range of the power consumed by cutting given by the experiments and the numerical model. This variation range is defined as the ratio of the difference between the maximum and minimum values to the mean average value. The obtained results are showed in Fig. 10. We note, for the experimental cutting power, a variation range equal to 2.16% and, for the numerical model, to 5.89%. This difference between the two ratios is explained by the fact we have neglected the table and spindle gearbox effects in our modelling, which caused a supplementary damping in the structure.

In the rest of the manuscript, we are interested in the mean average value of the consumed cutting power. A comparison between the experimental and computed cutting power and energy is performed for a single-pass face milling, using a four-tooth BDMT070304ERML face-milling cutter of 40 mm in diameter. We have examined the cutting energy and power for four study cases, as described by Table 4. For each case, we change the cutting speed, the axial depth of cut or the feed per tooth.

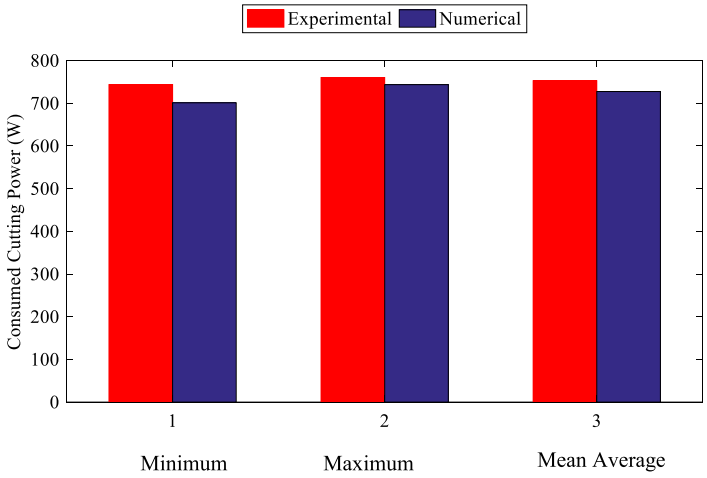

Fig. 9. Comparison between the computed and experimental minimum, maximum, and mean average values of the consumed power.

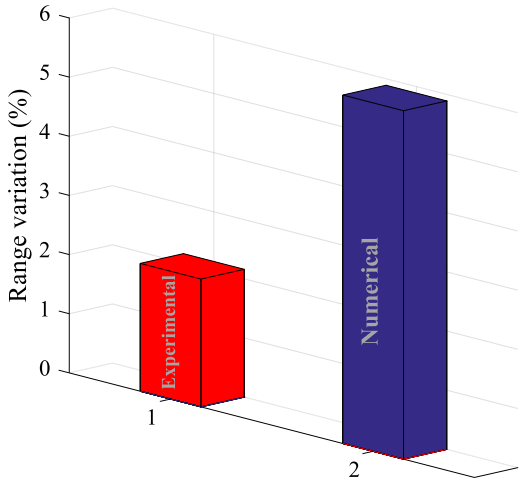

Fig. 10. Comparison of the range variation between the experimental and computed cutting power values.

Table 4
Different studied cases.

Case study order	Cutting speed V_c (m/min)	Axial depth of cut a_p (mm)	Feed per tooth f_z (mm/tooth)
First order	140	2	0.2
Second order	140	2	0.1
Third order	140	1	0.2
Fourth order	90	2	0.2

A reference case corresponds to a cutting speed of 140 m/min with an axial depth of cut equal to 2 mm and a feed per tooth equal to 0.2 mm/tooth. In the second case, we decrease the feed per tooth to 0.1 mm/tooth. This variation leads to a decrease in the cutting power, but, on the other hand, it increases the values of the cutting energy. These results are explained by the proportionality between the tangential cutting force and the feed per tooth, as shown by Eq. (9). Indeed, the cross section variation depends on the variation of the feed per tooth and consequently on a decrease of the cutting section.

Furthermore, this variation is relative to the effect of the instantaneous size of the chip thickness. From these results, we can note the importance of taking into account the instantaneous chip thickness in strengthening the evaluation of the variable cutting forces and consequently the evaluation of the required cutting power. In this study case, the cutting time is inversely proportional to the feed per tooth, which causes an augmentation of the cutting energy value. These results are compared with experiments where the error is between 3.36% and 4.9% for the cutting power and the energy, respectively (Fig. 12).

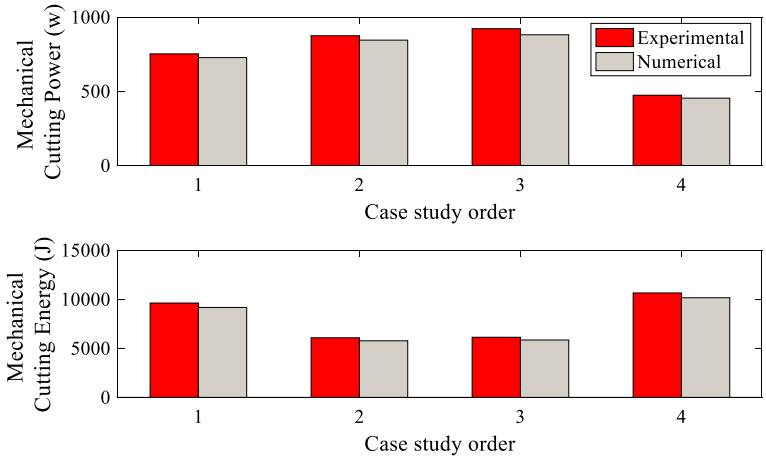

Fig. 11. Comparison of the experimental and computed results for a BDMT070304ERML face-milling cutter.

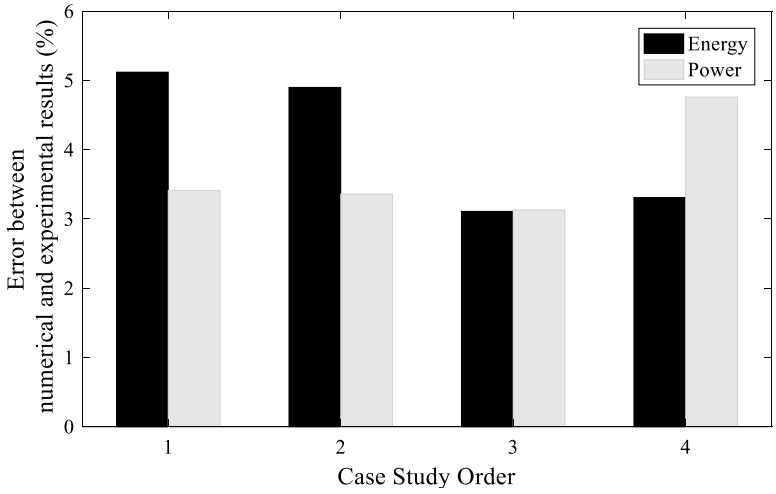

Fig. 12. Error between the computed and experimental results.

The third study case corresponds to a decrease in the axial depth of cut up to 1 mm, and the feed per tooth is fixed at 0.2 mm/tooth, which leads to a fall of the cutting energy and of the power, as shown in Fig. 11. In fact, the tangential cutting force of Eq. (9) is proportional to the axial depth, caused by a decrease in the width of the chip thickness. But the cutting time is independent of the axial depth of cut. These results are compared with experiments where the error is between 3.13% and 3.11% for the cutting power and the energy, as displayed in Fig. 12.

The last study case is obtained for a cutting speed of 90 m/min, a feed per tooth equal to 0.2 mm/tooth, and an axial depth of cut equal to 2 mm. A decrease with respect of the first study case is obtained. For the cutting power, we note that the power difference value reaches 13.5%, which is caused by the impact of the cutting speed on the cutting force. These results are compared with those of experiments where a good agreement is shown between the experimental and computed values of energy and power, where the error reaches about 3.31% and 4.76%, respectively.

This slight deviation is caused, in our opinion, by the progression of tool wear, which increases cutting energy consumption. Indeed, when the same cutting tool is used for several machining tests, its wear leads to the rise of the cutting forces and more energy consumption, as a consequence. This deviation can be also caused by the experimental set-up, which is not perfectly rigid.

For NC machines, the bearings power loss dominates the total mechanical loss of the spindle system [30], so we aim to study the impact of the bearings and their associated defect on the power consumed by the spindle.

In order to study the impact of the bearings on the spindle system's energy, we compute the bearings' energy during the approach phase, taking into consideration the fact that the cutting forces are equal to zero. The equation of motion is then resolved, and the energy is computed using the flowchart of Fig. 8. We compare the computed bearing energy with the experimental one, which is obtained by subtracting the energy from the total approach phase energy to accelerate the total moment of inertia. The following table summarizes the obtained results.

Table 5
Numerical and experimental power and energy of healthy bearings during the approach phase.

	Rotational spindle speed (rpm)	
	1115	716
Computed bearing energy (J)	587	362.5
Experimental bearing energy (J)	609.9	375.2
Error (%)	3.75	3.38
Computed bearing power (W)	119.6	69.12
Experimental bearing power (W)	123.61	71.92
Error (%)	3.24	3.89

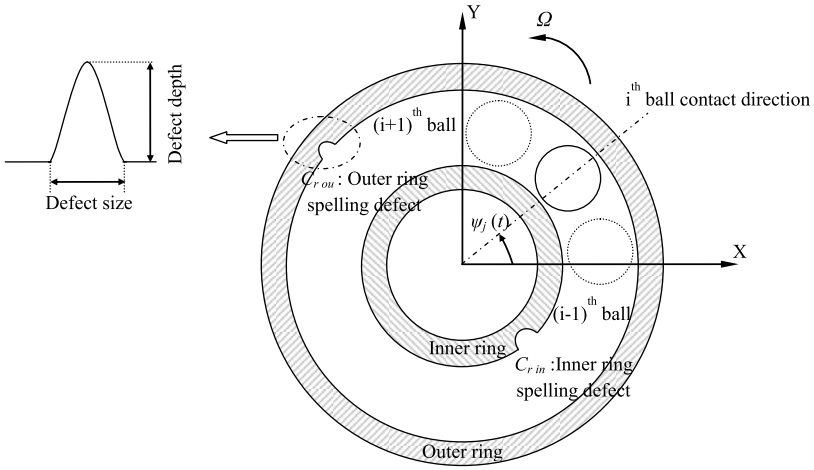

Fig. 13. Spalling defect of a bearing.

By examining Table 5, we note that the error between the computed and the experimental bearing energies ranges from (3.75%) to (3.38%) when the rotating speed is equal to 1115 rpm and 716 rpm, respectively. We note also that the energy of the bearings is proportional to the rotating speed. This result is illustrated in Fig. 14, which shows the variation of the computed energy of the bearings with the revolution speed. We note an increase of the bearing energy, explained by the impact of the rotating speed on the viscosity-related torque Eq. (21).

We introduce now in our model a spalling defect in the outer ring, as shown in Fig. 13. The defect, defined as a half of a sinus [25], having a size of $\frac{5\pi}{23}$ mm, a height of 3 µm and a null initial position, is introduced in Eq. (20), written as:

$$\Delta_j = d(\psi_j(t)) - d_0 - C_{\text{r in/ou}} \tag{22}$$

Fig. 14 shows clearly that the front bearing's spalling defect leads to an increase in the spindle's power losses during the approach phase, especially when the system's revolution speed becomes high. In fact, the power loss of the bearings is tripled when the speed of revolution ranges from 4000 rpm to 8000 rpm. We conclude that it is important to incorporate the power loss caused by the friction of the bearing system and the associated defects during the estimation of the power consumed by the spindle.

In order to show the impact of the outer ring spalling defect dimensions on the power consumed by the spindle during the approach phase, a parametric study has been performed, in which we changed the defect height and size values; the obtained results for a speed of revolution equal to 4000 rpm are given in Table 6.

The results show that, during the approach phase, an increase of the power consumed by spindle is achieved with the increase of the defects' height and size values. Indeed, when the spalling is more extended, the spindle useful torque is increased in order to overcome this defect, while causing slight malfunctions. In order to study the impacts of the inner and outer rings defects on the power consumed by spindle, a parametric study is performed, giving the variation of the spindle power with respect to the outer ring defect, the inner ring defect and the combined inner and outer rings defects for different defect height values. The defect size is fixed for the outer and inner rings as $\frac{4\pi}{23}$. The obtained results for a speed of revolution of 4000 rpm are shown in Figs. 15 and 16.

Fig. 15 and 16 show that the presence of a defect at both the inner and the outer rings leads to an increase of the power consumed by the spindle system during the approach phase. For an inner ring defect, the increase of the consumed power is larger than that of the outer ring defect, despite the similarity of the defect dimensions. In fact, the outer ring is considered fixed, but the inner ring is in revolution. Thus, the existence of a spalling defect in the inner ring will cause more vibrations

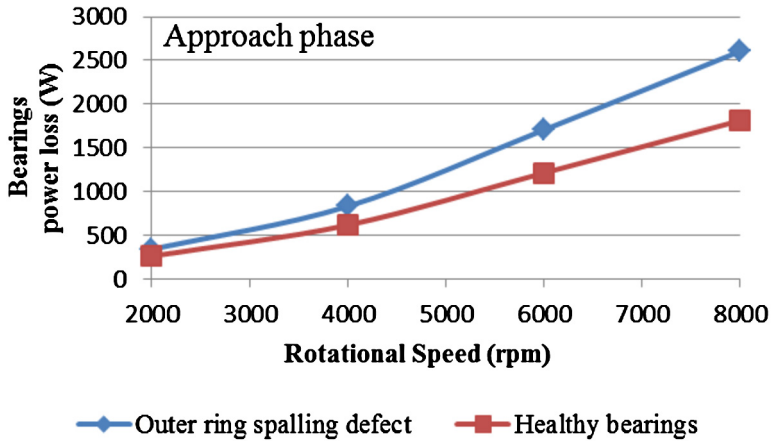

Fig. 14. Impact of the revolution speed on the bearings' energy during the approach phase.

Table 6
Power consumed by the spindle (W) during the approach phase for different values of the outer ring spalling defect.

		Defect height (μm)		
		2.5	3	3.5
Defect size (mm)	$\frac{4\pi}{23}$	701.8	740.2	789.7
	$\frac{5\pi}{23}$	755.5	822.8	881.4
	$\frac{6\pi}{23}$	837	917.6	1015

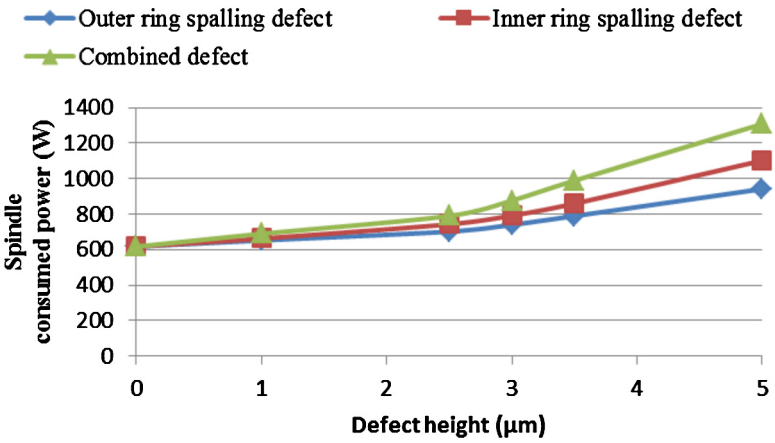

Fig. 15. Impact of the inner and outer spalling defect on the power consumed by the spindle during the approach phase.

in the spindle system, as illustrated in Fig. 16. These vibrations need a spindle useful torque much higher than in the case of the outer ring to overcome this defect and the associated vibrations. These figures show also an exponential increase of the consumed power with respect to the defect height. In fact, for an increase of 0.5 μm of the defect height, we pass from a rate of increase of 38.4% (defect height range from 2.5 μm to 3 μm) in a first time and a rate of increase of 49.5% (defect height range from 3 μm to 3.5 μm) in a second time, as shown in Fig. 16.

When we examine the FFT of the first node radial displacement, we note the presence of the cage frequency ($f_c = 30.93$ Hz) corresponding to the temporal variation of the external load, which varies periodically for each bearing round. We note also the presence of the ball passage frequency ($f_{pb} = N_b f_c = 703$ Hz), corresponding to the passage from a ball to the next one. For the inner ring defect spectrum, we note the presence of the characteristic defect frequency ($f_{id} = f_i - f_c$) and a modulation between the defect frequency and the rotational spindle frequency and the cage rotation frequency. An increase of the vibratory level is noted when we pass from a healthy system spectrum to an outer defect system spectrum in a first time and to an inner defect system spectrum in a second time, which explains the increase of the power consumed by the spindle, as shown in Fig. 17.

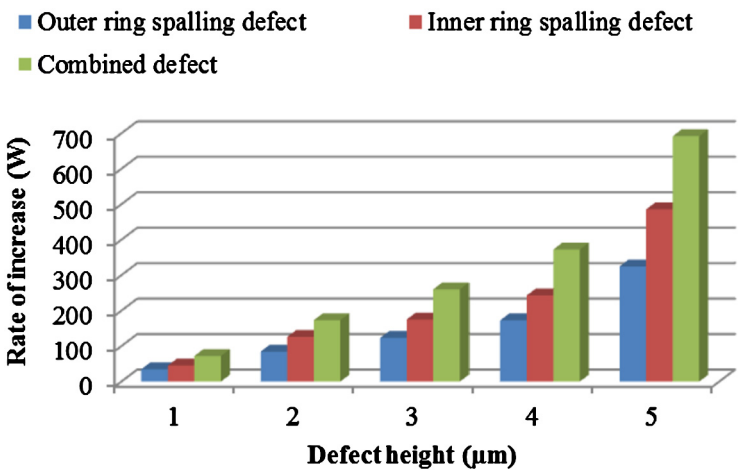

Fig. 16. Rate of increase of the power consumed by the spindle.

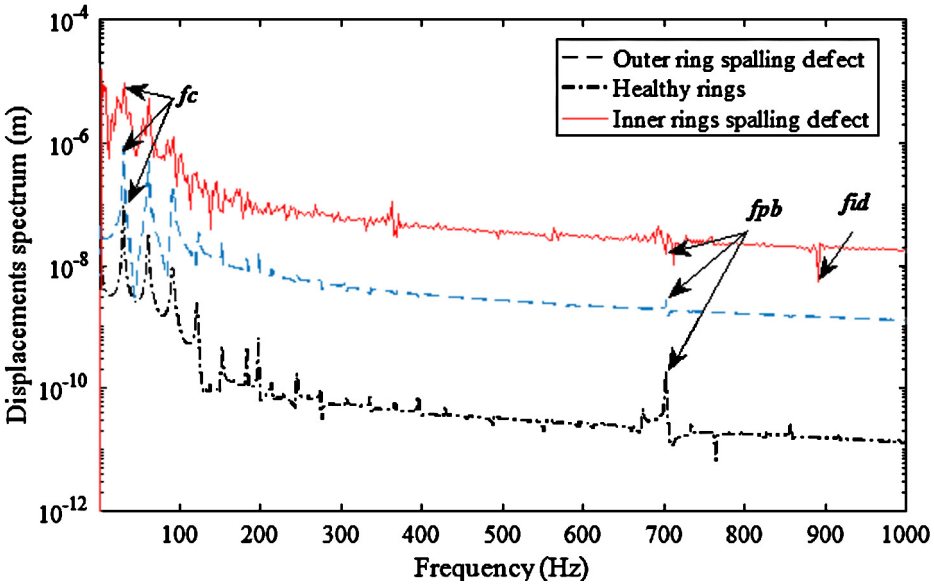

Fig. 17. Spectrum with and without defect of the first-node radial displacement.

We introduce also an eccentricity defect on the front bearing. This defect is characterized by the eccentricity radius r, as given in Fig. 18 [31]. The eccentricity defect $\delta(\psi_j)$ is given as an additional term in the angular position of the jth ball as:

$$\delta(\psi_j) = \frac{2r}{d_m}\cos(\psi_j) \tag{23}$$

A parametric study is performed for this defect type and the results are given in Table 7.

When we examine these results, we note an increase in the consumed power with increasing eccentricity. In fact the motor useful torque is increased to overcome the malfunctions of the spindle system caused by eccentricity.

An unbalance defect is included in our model, defined as an excitation force F_b added in the second member of the equation of motion – Eq. (6) – as proposed by Hentati [25]. This unbalance excitation is written using the unbalance mass m_b, the spindle angular velocity and the unbalance vector distribution as given in Hentati [25]. We choose an unbalance mass value equal to 4×10^{-4} kg. The power consumed by the spindle is then calculated.

A comparison between the computed power consumed by the spindle for different defect types and that consumed by a spindle working during the approach and cutting phases (rotating at 4000 rpm with a feed rate equal to 0.2 mm/tooth and axial depth equal to 1 mm) is summarized in Table 8.

We note from Table 8 that the rate of increase is more important for the spalling defect. We can conclude that the mounting faults (eccentricity and unbalance) do not have a great impact on the consumed power. On the other hand, the wear defect (inner and outer rings spalling) causes a significant increase of the consumed power, which varies with the

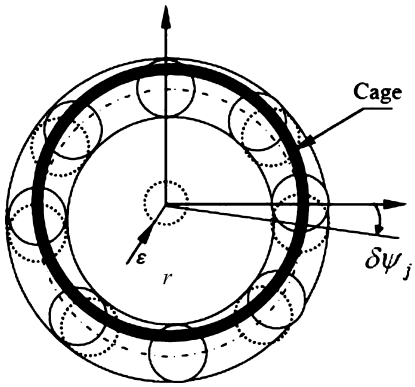

Fig. 18. Spacing between the balls in the case of eccentricity of the cage defect [31].

Table 7
Variation of the power consumed by the spindle during the approach functioning of an eccentricity radius defect.

Eccentricity radius (mm)	Spindle consumed power (W)
0	617.38
1	708.7
2	724.5
3	752.3

Table 8
Numerical spindle consumed power for different types of defects in the approach and cutting phases.

		Without defect	Inner ring spalling defect	Outer ring spalling defect	Eccentricity defect	Unbalance defect
Approach phase	Computed power consumed by the spindle (W)	617.38	868.1	822.8	708.7	762.8
	Rate of increase (%)	–	28.88	24.96	12.88	19.06
Cutting phase	Computed power consumed by the spindle (W)	2022	2894	2761	2496.1	2648
	Rate of increase (%)	–	30.13	26.76	18.99	23.64

dimensions of the spalling. These results are confirmed for both phases, especially for a spindle in the cutting phase, where the rate of increase of the consumed power can reach 30.13%.

5. Conclusion

In this investigation, we propose a numerical model that we apply to a milling machine tool in order to estimate the power and the energy consumed by the spindle during the approach and the cutting phases in the presence of different defect types.

The proposed model takes into account the dynamic response of the milling cutting force and the dynamic behavior of the bearing force.

A parametric study is performed to show the variation of the consumed power with respect with cutting parameters such as the cutting speed, the axial depth of cut, and the feed per tooth. The obtained results are compared with the experiments. We can conclude from the parametric study that a good selection of cutting parameters leads a reduction of the power consumed by the spindle.

We were also interested in studying the impact of mounting faults and wear faults on the consumed power during the approach and cutting phases. For mounting faults, we have chosen eccentricity and unbalance, and for wear faults, we have chosen inner and outer rings spalling defects. The obtained results show that the wear defects have a more important increase on the consumed power than the mounting ones, especially for inner ring spalling and for important rotating speed where the rate of increase can reach 30%. These results emphasize the preventive maintenance, which leads to an important reduction of the consumed power. Also, for a milling spindle working at higher rotational speed, we can conclude that rotational guidance is better when it is insured by magnetic bearings rather by ball bearings.

This approach can be used to optimize the energy and the power consumed by the spindle in the milling process.

References

[1] T.G. Gutowski, J.M. Allwood, C. Herrmann, S. Sahni, A global assessment of manufacturing: economic development, energy use, carbon emissions, and the potential for energy efficiency and materials recycling, Annu. Rev. Env. Resour. 38 (2013) 81–106.
[2] L. Zhou, J. Li, F. Li, Q. Meng, J. Li, X. Xu, Energy consumption model and energy efficiency of machine tools: a comprehensive literature review, J. Clean. Prod. 112 (2016) 3721–3734.
[3] S.T. Newman, A. Nassehi, R. Imani-Asrai, V. Dhokia, Energy efficient process planning for cnc machining, CIRP J. Manuf. Sci. Technol. 5 (2) (2012) 127–136.
[4] F. Liu, Q. Wang, G. Liu, Content architecture and future trends of energy efficiency research on machining systems, J. Mech. Eng. 49 (19) (2013) 87–94.
[5] Y. He, B. Liu, X. Zhang, H. Gao, X. Liu, A modeling method of task-oriented energy consumption for machining manufacturing system, J. Clean. Prod. 23 (1) (2012) 167–174.
[6] G. Kant, K.S. Sangwan, Prediction and optimization of machining parameters for minimizing power consumption and surface roughness in machining, J. Clean. Prod. 83 (2014) 151–164.
[7] W. Li, S. Kara, An empirical model for predicting energy consumption of manufacturing processes: a case of turning process, Proc. Inst. Mech. Eng., B J. Eng. Manuf. 225 (9) (2011) 1636–1646.
[8] W. Lee, S.H. Kim, J. Park, B.-K. Min, Simulation-based machining condition optimization for machine tool energy consumption reduction, J. Clean. Prod. 150 (2017) 352–360.
[9] L. Hu, C. Peng, S. Evans, T. Peng, Y. Liu, R. Tang, A. Tiwari, Minimising the machining energy consumption of a machine tool by sequencing the features of a part, Energy 121 (2017) 292–305.
[10] S. Jia, R. Tang, J. Lv, Z. Zhang, Q. Yuan, Energy modeling for variable material removal rate machining process: an end face turning case, Int. J. Adv. Manuf. Technol. 85 (9–12) (2016) 2805–2818.
[11] F. Liu, Z. Xu, B. Dan, et al., Energy Characteristics of Machining Systems and Its Application, China Machine Press, Beijing, 1995.
[12] A. Dietmair, A. Verl, Energy consumption forecasting and optimisation for tool machines, Energy 62 (2009) 63.
[13] S. Hu, F. Liu, Y. He, B. Peng, Characteristics of additional load losses of spindle system of machine tools, J. Adv. Mech. Des. Syst. Manuf. 4 (7) (2010) 1221–1233.
[14] T. Peng, X. Xu, An interoperable energy consumption analysis system for cnc machining, J. Clean. Prod. 140 (2017) 1828–1841.
[15] O.I. Avram, P. Xirouchakis, Evaluating the use phase energy requirements of a machine tool system, J. Clean. Prod. 19 (6–7) (2011) 699–711.
[16] J. Lv, R. Tang, S. Jia, Y. Liu, Experimental study on energy consumption of computer numerical control machine tools, J. Clean. Prod. 112 (2016) 3864–3874.
[17] X. Ai, S. Xiao, Concise Manual of Cutting Parameters, China Machine Press, Beijing, 1994.
[18] Z. Deng, H. Zhang, Y. Fu, L. Wan, W. Liu, Optimization of process parameters for minimum energy consumption based on cutting specific energy consumption, J. Clean. Prod. 166 (2017) 1407–1414.
[19] C. Li, X. Chen, Y. Tang, L. Li, Selection of optimum parameters in multi-pass face milling for maximum energy efficiency and minimum production cost, J. Clean. Prod. 140 (2017) 1805–1818.
[20] F. Draganescu, M. Gheorghe, C. Doicin, Models of machine tool efficiency and specific consumed energy, J. Mater. Process. Technol. 141 (1) (2003) 9–15.
[21] M. Rief, B. Karpuschewski, E. Kalhöfer, Evaluation and modeling of the energy demand during machining, CIRP J. Manuf. Sci. Technol. 19 (2017) 62–71.
[22] S. Borgia, P. Albertelli, G. Bianchi, A simulation approach for predicting energy use during general milling operations, Int. J. Adv. Manuf. Technol. 90 (9–12) (2017) 3187–3201.
[23] I.F. Edem, P.T. Mativenga, Modelling of energy demand from computer numerical control (CNC) toolpaths, J. Clean. Prod. 157 (2017) 310–321.
[24] J. Lv, T. Peng, R. Tang, Energy modeling and a method for reducing energy loss due to cutting load during machining operations, Proc. Inst. Mech. Eng., B J. Eng. Manuf. (2018) 0954405418769922.
[25] T. Hentati, M. Barkallah, S. Bouaziz, M. Haddar, Dynamic modeling of spindle-rolling bearings systems in peripheral milling operations, J. Vibroeng. 18 (3) (1982).
[26] A. Ben Jdidia, A. Bellacicco, T. Hentati, M. Barkallah, M.T. Khabou, A. Rivier, M. Haddar, Modelling of axis feed consumed energy for sustainable manufacturing, J. Chin. Inst. Eng. 42 (5) (2019) 377–384.
[27] E. Budak, Analytical models for high performance milling. Part I: Cutting forces, structural deformations and tolerance integrity, Int. J. Mach. Tools Manuf. 46 (12–13) (2006) 1478–1488.
[28] I.O. Avram, Machine Tool Use Phase: Modeling and Analysis with Environmental Considerations, Ph.D. thesis, École polytechnique fédérale de Lausanne, Lausanne, Switzerland, 2010.
[29] FAG, Super precision bearings: catalogue, https://www.schaeffler.com/remotemedien/media/_shared_media/08_media_library/01_publications/schaeffler_2/brochure/downloads_1/ac_41130_7_de_en.pdf.
[30] T. Holkup, H. Cao, P. Kolář, Y. Altintas, J. Zelený, Thermo-mechanical model of spindles, CIRP Ann. 59 (1) (2010) 365–368.
[31] T. Hentati, Contribution à l'étude dynamique d'un palier à roulement en présence de défauts, PhD thesis, École nationale d'ingénieurs de Sfax, Sfax, Tunisia, 2008.